as follows. Conidial structure of the strain was biseriate and similar to that of *Aspergillus*. Sterigmata were shaped like an ampule with short a neck. Conidiophores were smooth, extremely short (40~80×2.5~3.0 μm), colorless, with foot cells and with vesicle (sub-rounding to flask shape, 10~15 μm i.d.) at the apex. Metulae were not found. Phialides grew from upper half of the vesicle to upper side, and were 6.0~7.5×1.8~2.5 μm in size. Conidia were one-celled, rounded, 2.5~3.5 μm i.d., smooth in the surface and formed connected to each other like a chain. Hülle cells and chlamydospores were not observed. Sexual reproduction organs such as cleistoyhecium were not found when the culture was observed for over four weeks.

These cultural and morphological characteristics suggest that the strain should be included in the genus *Aspergillus*. However, the properties mentioned above did not agree with those of any known species in the genus. Then, we classified this isolate as one strain of *Aspergillus*, and named it *Aspergillus* sp. F-1491. It was deposited at the National Institute of Bioscience and Human-Technology, Agency of Industrial science and Technology, Japan as FERM P-18549.

Fig. 2. Scanning electron micrograph of strain F-1491 (on the potato dextrose agar plate at 25°C).

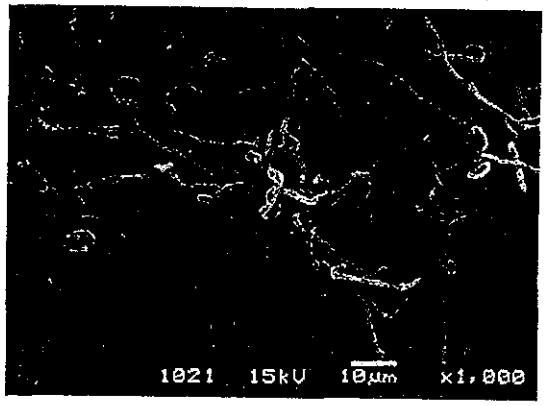

Isolation and Purification

The isolation procedure of ICM0301s is shown in Fig. 3. After the fermentation, broth (130 liters) was filtered and the mycelium was extracted with MeOH (15 liters). The filtrate was adsorped on a Diaion HP-20 column (5 liters) and washed with 20% MeOH (10 liters). Active ingredients were eluted by MeOH (15 liters) and combined with the mycelial extract. The solution was concentrated, and resulting aqueous solution was extracted with EtOAc (5 liters). The organic layer was washed with water, dried over Na_2SO_4 and concentrated *in vacuo* to give an oily material (80 g). This was dissolved in a small volume of $CHCl_3$, and applied on a silica gel column (3 liters, dry volume). After washing with $CHCl_3$ (5 liters), **1**, **2**, **3**, **4**, **5**, **6** and **7** were eluted with $CHCl_3$-MeOH (25:1, 5 liters), and **8** was

Fig. 3. Isolation procedure for ICM0301s.

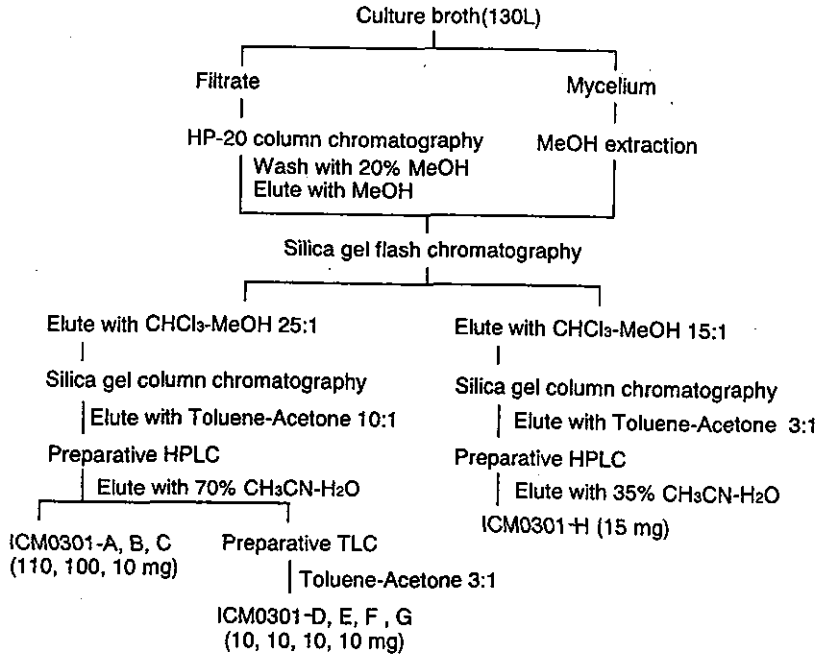

further eluted with $CHCl_3$-MeOH (15 : 1, 5 liters). The fractions containing **1** to **7** were dissolved in a small volume of toluene and applied on a silica gel column (400 ml). After washing with toluene-acetone (20 : 1, 1 liter), active ingredients were eluted with toluene-acetone (10 : 1, 1 liter). This fraction was concentrated *in vacuo* to give a yellow powder (1.2 g). This powder was dissolved in a small volume of MeOH and applied on a preparative HPLC column. Active ingredients were eluted with 70% acetonitrile at a flow rate of 7 ml/minute. Compounds **1**, **2** and **3** were separately eluted in this order to give **1** (110 mg), **2** (100 mg), **3** (10 mg) as white powders, respectively. Compounds **4** and **5**, **6** and **7** were eluted as mixture. Further purification was carried out by preparative TLC (toluene-acetone 3 : 1) to give **4** (10 mg), **5** (10 mg), **6** (10 mg) and **7** (10 mg) as white powders, respectively. The fraction containing **8** was dissolved in a small volume of toluene and applied on a silica gel column (400 ml). After washing with toluene-acetone (5 : 1, 1 liter), active ingredients were eluted with toluene-acetone (3 : 1, 1 liter) to give a yellow powder (0.8 g). This powder was applied on a preparative HPLC, and eluted with 35% acetonitrile at a flow rate of 7 ml/minute to give **8** (15 mg) as a white powder.

The retention time and Rf value of ICM0301s are summarized in Table 2.

Physico-chemical properties and structure elucidation of ICM0301s will be described in a following paper.

Table 2. Retention times and Rf values of ICM0301s.

Compounds	Retention time (min.)*	Rf value**
ICM0301A	10.8	0.67
B	7.3	0.61
C	11.3	0.46
D	7.7	0.42
E	7.8	0.37
F	5.3	0.48
G	5.1	0.56
H	2.8	0.38

* Mobile phase: 50 % acetonitrile-H_2O

** TLC plate: Merck Art. 5715

Solvent systems: toluene-acetone 4:1 (A~E), 2:1 (F~H)

Growth Inhibitory Activities against Human Cells

Growth inhibitory activities of ICM0301s against HUVECs and human tumor cell lines were assessed. As shown in Table 3, ICM0301s showed potent inhibitory activities against HUVECs. Among them, ICM0301A (**1**) showed the strongest inhibitory activity against HUVECs with IC_{50} value of 2.2 μg/ml.

On the other hand, ICM0301s had no significant cytotoxic activities at 100 μg/ml against human tumor cell lines including H226, DLC-1, HT-1080. ICM0301s showed weak cytotoxicities against K562 cells.

Anti-angiogenic Activities in Rat Aorta Organ Culture

Anti-angiogenic activity of ICM0301A (**1**) was assessed by using the *in vitro* angiogenesis model of culturing fragment of rat aorta in three-dimensional fibrin gels. As shown in Fig. 4, **1** exhibited dose dependent anti-angiogenic activity, and showed significant inhibitory activity of 52% inhibition at 1 μg/ml. Angiogenesis was completely inhibited at 10 μg/ml. Fumagillin, a potent angiogenesis inhibitor through methinone amino-peptidase inhibition[19], showed complete inhibition at 10 ng/ml. It is known that anti-proliferative agents against ECs, MMP inhibitors[20], hydrocortisone[17], and endogenous

Table 3. Growth inhibitory activities of ICM0301s against HUVECs and human tumor cell lines.

Cells	IC_{50} (μg/ml)							
	A	B	C	D	E	F	G	H
HUVEC	2.2	3.2	7.4	4.6	3.2	9.3	7.7	5.6
K562	39	36	52	80	68	72	95	61
H226	>100	>100	>100	>100	>100	>100	>100	>100
DLD-1	>100	>100	>100	>100	>100	>100	>100	>100
HT1080	>100	>100	>100	>100	>100	>100	>100	>100

Fig. 4. Anti-angiogenic activity of ICM0301A on rat aorta organ culture.

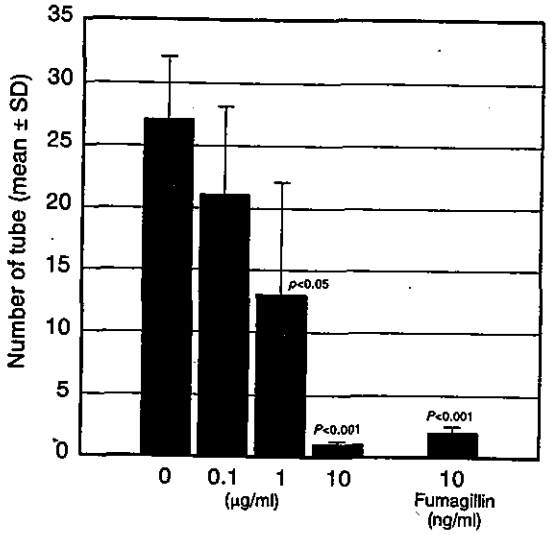

angiogenesis inhibitors[21] exhibit anti-angiogenic activity in this model. Anti-angiogenic activity of **1** may be mainly exhibited through its anti-proliferative activity against ECs. Since angiogenesis in this model has occurred without supplement of serum and growth factors, this assay bridges the gap between *in vitro* and *in vivo* models combining advantages of both systems. Then, effectiveness of **1** in the *in vitro* model may be expected to follow through into *in vivo* angiogenesis models.

Anti-microbial Activity and Toxicity in Mice

Because fusarielin A[19], a compound structurally related to ICM0301s, was reported to show an MIC value of 3.1 μg/ml against *Aspergillus fumigatus* 11268, ICM0301s were expected to have anti-fungal activities. However, ICM0301s had no anti-fungal activity at 100 μg/ml.

Toxicity of **1** against mice was assessed. Body weight changes of mice given 100 mg/kg of **1** was equal to that of control mice for 2 weeks after intraperitoneal injection.

From the results mentioned above, ICM0301s may be useful in human diseases such as solid tumor and rheumatoid arthritis by virtue of its anti-angiogenic activity.

References

1) FOLKMAN, J. & P. A. D'AMORE: Blood vessel formation: what is its molecular basis? Cell 87(7): 1153~1155, 1996
2) FOLKMAN, J. & Y. SHING: Angiogenesis. J. Biol. Chem. 267(16): 10931~10934, 1992
3) FOLKMAN, J.: The role of angiogenesis in tumor growth Semin Cancer Biol. 3(2): 65~71, 1992
4) WEIDNER, N.; P. R. CARROLL, J. FLAX, W. BLUMENFELD & J. FOLKMAN: Tumor angiogenesis correlates with metastasis in invasive prostate carcinoma. Am. J. Pathol 143(2): 401~409, 1993
5) GIATROMANOLAKI, A.; E. SIVRIDIS, N. ATHANASSOU, E. ZOIS, P. E. THORPE, R. A. BREKKEN, K. C. GATTER, A. L. HARRIS, I. M. KOUKOURAKIS & M. I. KOUKOURAKIS: The angiogenic pathway "vascular endothelial growth factor/flk-1 (KDR)-receptor" in rheumatoid arthritis and osteoarthritis. J. Pathol. 194(1): 101~108, 2001
6) HANAHAN, D.: Signaling vascular morphogenesis and maintenance. Science 277: 48~50, 1997
7) RISAU, W.: Mechanism of angiogenesis. Nature 386(17): 671~674, 1997
8) YANASE, T.; M. TAMURA, K. FUJITA, S. KODAMA & K. TANAKA: Inhibitory effect of angiogenesis inhibitor TNP-470 on tumor growth and metastasis of human cell lines *in vitro* and *in vivo*. Cancer Res. 53(11): 2566~2570, 1993
9) ASANO, M.; A. YUKITA & H. SUZUKI: Wide spectrum of antitumor activity of a neutralizing monoclonal antibody to human vascular endothelial growth factor. Jpn. J. Cancer Res. 90(1): 93~100, 1999
10) AONUMA, M.; Y. YOSHITAKE, K. NISHIKAWA & N. G. TANAKA: Different antitumor activities of anti-bFGF neutralizing antibodies: heparin-binding domain provides an inefficient epitope for neutralization *in vivo*. Anticancer Res. 19(5B): 4039~4044, 1999
11) BROOKS, P. C.; A. M. MONTGOMERY, M. ROSENFELD, R. A. REISFELD, T. HU, G. KLIER & D. A. CHERESH: Integrin alpha v beta 3 antagonists promote tumor regression by inducing apoptosis of angiogenic blood vessels. Cell. 79(7): 1157~1164, 1994
12) ALLMAN, R.; P. COWBURN & M. MASON: *In vitro* and *in vivo* effects of a cyclic peptide with affinity for the alpha(nu) beta3 integrin in human melanoma cells. Eur. J. Cancer 36(3): 410~422, 2000
13) TILLE, J. C.; J. WOOD, S. J. MANDRIOTA, C. SCHNELL, S. FERRARI, J. MESTAN, Z. ZHU, L. WITTE & M. S. PEPPER: Vascular endothelial growth factor (VEGF) receptor-2 antagonists inhibit VEGF- and basic fibroblast growth factor-induced angiogenesis *in vivo* and *in vitro*. J. Pharmacol. Exp. Ther. 299(3): 1073~1085, 2001
14) PITT, J. I.: The genus *Penicillium* and its teleomorphic states *Eupenicillium* and *Talaromyces*. Academic Press, London, 1979
15) CARMICHAEL, J. W.; W. B. KENDRIC, I. L. CONNERS & L. SIGLER: Genera of Hyphomycetes. University of Alberta Press, Alberta, 1980
16) KORNERUP, A. & J. H. WANSCHER: Methuen handbook of color, 3rd ed., Eyre Methuen, London, 1978
17) NICOSIA, R. F. & A. OTTINETTI: Growth of microvessels in serum-free matrix culture of rat aorta: A quantitative assay of angiogenesis *in vitro*. Lab. Invest. 63: 115~122, 1990
18) SIN, N.; L. MENG, M. Q. WANG, J. J. WEN, W. G. BORNMANN & C. M. CREWS: The anti-angiogenic agent fumagillin covalently binds and inhibits the methionine aminopeptidase, MetAP-2. Proc. Natl. Acad. Sci. 94(12): 6099~6103, 1997

19) KOBAYASHI, H.; R. SUNAGA, K. FURIHATA, N. MORISAKI & S. IWASAKI: Isolation and structures of an antifungal antibiotic, fusarielin A, and related compounds produced by a *Fusarium* sp. J. Antibiotics 48(1): 42~52, 1995

20) ZHU, W. H.; X. GUO, S. VILLASCHI & R. F. NICOSIA: Regulation of vascular growth and regression by matrix metalloproteinases in the rat aorta model of angiogenesis. Lab. Invest. 80(4): 545~555, 2000

21) ERGUN, S.; N. KILIC, J. H. WURMBACH, A. EBRAHIMNEJAD, M. FERNANDO, S. SEVINC, E. KILIC, F. CHALAJOUR, W. FIEDLER, H. LAUKE, K. LAMSZUS, P. HAMMERER, J. WEIL, H. HERBST & J. FOLKMAN: Endostatin inhibits angiogenesis by stabilization of newly formed endothelial tubes. Angiogenesis 4(3): 193~206, 2001

VOL. 57 NO. 2, FEB. 2004 THE JOURNAL OF ANTIBIOTICS pp. 104 — 109

ICM0301s, New Angiogenesis Inhibitors from *Aspergillus* sp. F-1491

II. Physico-chemical Properties and Structure Elucidation

TETSUYA SOMENO*, HIROYUKI KUMAGAI, SHUN-ICHI OHBA, MASAHIDE AMEMIYA, HIROSHI NAGANAWA, MASAAKI ISHIZUKA and DAISHIRO IKEDA*

Microbial Chemistry Research Center
Numazu Bio-Medical Research Institute
18-24 Miyamoto, Numazu-shi, Shizuoka 410-0301, Japan

(Received for publication September 26, 2003)

ICM0301A (**1**), B (**2**) and their congeners (**3**~**8**) were isolated from a culture broth of *Aspergillus* sp. F-1491 as new angiogenesis inhibitors. Their structures were elucidated by spectroscopic analyses. ICM0301A and B have a substituted decalin skeleton containing two oxirane rings.

In the course of our screening for new angiogenesis inhibitors[1~3] from microbial products, we have isolated eight new structurally related compounds from a culture broth of *Aspergillus* sp. F-1491. The taxonomy of the producing strain and fermentation, isolation, and biological activities of ICM0301s are reported in the preceding paper[4]. In this paper, we describe the physico-chemical properties and structure elucidation of ICM0301s.

Results and Discussion

Physico-chemical Properties of ICM0301s

ICM0301s were isolated as white powders. Among them, ICM0301A (**1**) and B (**2**) were obtained as major products. The physico-chemical properties of **1** and **2** are summarized in Table 1. The UV spectra of all ICM0301s in MeOH exhibited essentially the same absorption maxima at 280 nm. Their IR spectra showed a ν_{max} at around 1660 cm^{-1}. These observations suggested the presence of a conjugated dienone system.

Structure Elucidation of ICM0301 A (1)

The molecular formula of ICM0301A (**1**) was determined to be $C_{24}H_{34}O_3$ by HRFAB-MS, HRESI-MS and ^{13}C NMR analyses. The degree of unsaturation was calculated to be eight by its molecular formula. Since the ^1H and ^{13}C NMR spectra of **1** in CD_3OD at room temperature displayed broad signals, NMR experiments were carried out at 40°C. The ^1H NMR and HSQC spectra of **1** revealed 34 protons indicating the absence of hydroxyl group in the molecule.

The connectivity of two side chains (C-1~C-7 and C-18~C-20) was established by ^1H-^1H COSY with an aid of HMBC as shown in Fig. 2a. A substituted decalin moiety was elucidated as follow. The presence of two oxymethine carbons C-11 (δ_C 61.3), C-15 (δ_C 64.5) and two oxygenated quaternary carbons C-12 (δ_C 60.2), C-16 (δ_C 62.5) was suggested by the chemical shifts. This implies that each two of these carbons must form two ether moieties. Furthermore, large C-H coupling constants for sp^3 oxymethine carbons at C-11 ($^1J_{C\text{-}H}$=175 Hz) and C-15 ($^1J_{C\text{-}H}$=172 Hz) indicated the presence of two oxirane rings[5]. In the remaining part (tentatively C-8~C-17), no more double bond exists in the molecule based on the ^{13}C NMR spectrum. Taking the degree of unsaturation into consideration, two ring systems besides two oxirane rings should be formed by the remainder. In the ^1H-^1H COSY spectrum of **1**, sequential proton networks were observed within H-11, 10, 9, 8, 17 and H-14, 13 through H-9. In the HMBC spectrum, cross peaks were observed from methyl

* Corresponding author: numazu@bikaken.or.jp

Fig. 1. Relative structures of ICM0301s.

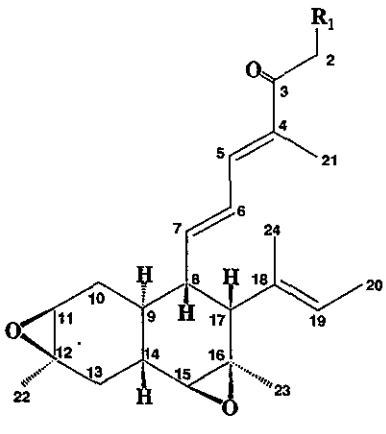

ICM0301A (1) R_1=CH_3
ICM0301B (2) R_1=H

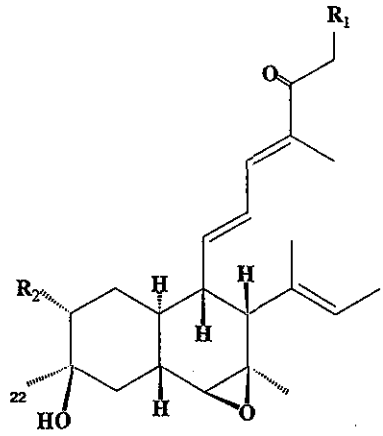

ICM0301C (3) R_1=CH_3, R_2=Cl
ICM0301D (4) R_1=H, R_2=Cl
ICM0301E (5) R_1=CH_3, R_2=H
ICM0301F (6) R_1=H, R_2=H
ICM0301G (7) R_1=H, R_2=OCH_3
ICM0301H (8) R_1=H, R_2=OH

Table 1. Physico-chemical properties of ICM0301A (1) and B (2).

	ICM 0301A(1)	ICM 0301B(2)
Appearance	White powder	White powder
Molecular formula	$C_{24}H_{34}O_3$	$C_{23}H_{32}O_3$
HRESI-MS(*m/z*)		
Observed	393.2406$(M+Na)^+$	379.2246$(M+Na)^+$
Calcd.	393.2406 for $C_{24}H_{34}O_3Na$	379.2249 for $C_{23}H_{32}O_3Na$
HRFAB-MS(*m/z*)		
Observed	371.2580$(M+H)^+$	357.2463$(M+H)^+$
Calcd.	371.2586 for $C_{24}H_{35}O_3$	357.2430 for $C_{23}H_{33}O_3$
$[\alpha]_D^{26}$	-194° (*c* 0.1, MeOH)	-222° (*c* 0.1, MeOH)
UV; λ(MeOH), nm(ε)	280 (26200)	280 (27500)
IR; ν cm^{-1}(KBr)	2970, 2915, 1660, 1630, 1440, 1375, 1260, 835	2965, 2925, 1655, 1630, 1435, 1375, 1255, 835

protons (H-22) to one quaternary carbon (C-12, δ_C 60.2), one methylene carbon (C-13, δ_C 36.8), one methine carbon (C-11, δ_C 61.3) and from H-23 to one quaternary carbon (C-16, δ_C 62.5), two methine carbons (C-15, δ_C 64.5 and C-17, δ_C 54.8), respectively. Cross peaks were also observed from H-15 to C-13 and C-14. These facts indicated the connectivity between C-11 and C-12, and between C-15 and C-16, respectively, resulting in the presence of substituted decalin ring. Cross peaks were observed from a methine proton (H-8) to C-7 and C-6 indicating that the long side chain should be attached at the C-8 position. Furthermore, cross peaks were observed from methyl protons of H-24 to C-17. Thus, the total planar structure of **1** was determined as shown in Fig. 2a.

The relative stereochemistry of **1** was elucidated by NOE difference and NOESY experiments (Fig. 2b). A large

Table 2. ^{1}H NMR data for **1**~**8**.

No	ICM0301A(1)[a]	ICM0301B(2)[a]	ICM0301C(3)[b]	ICM0301D(4)[c]
1	1.07 (3H, t, J=7.3)	-	1.06 (3H, t, J=7.4)	-
2	2.73 (2H, q, J=7.3)	2.31 (3H, s)	2.74 (2H, q, J=7.4)	2.30 (3H, s)
5	7.09 (1H, d, J=11.0)	7.12 (1H, d, J=11.0)	7.12 (1H, d, J=11.0)	6.94 (1H, d, J=11.0)
6	6.45 (1H, dd, J=15.0, 11.0)	6.46 (1H, dd, J=15.0, 11.0)	6.45 (1H, dd, J=15.0, 11.0)	6.33 (1H, dd, J=15.0, 11.0)
7	5.77 (1H, dd J=15.0, 10.0)	5.80 (1H, dd, J=15.0, 10.3)	5.78 (1H, dd, J=15.0, 10.5)	5.69 (1H, dd, J=15.0, 10.5)
8	2.29 (1H, ddd, J=11.0, 10.0, 5.0)	2.30 (1H, ddd, J=10.7, 10.3, 5.1)	2.40 (1H,ddd, J=11.0, 10.5, 5.0)	2.40 (1H, m)
9	1.38 (1H, m)	1.40 (1H, m)	2.05 (1H, m)	2.00 (1H,m)
10	1.13 (1H, dd, J=15.0, 12.0)	1.13 (1H, dd, J=15.0, 12.2)	1.62 (1H, m)	1.60 (1H, m)
	1.82 (1H, ddd, J=15.0, 5.6, 5.5)	1.82 (1H, ddd, J=15.0, 5.6, 5.5)	1.68 (1H, m)	1.68 (1H, m)
11	2.95 (1H, d, J=5.6)	2.98 (1H, d, J=5.6)	3.94 (1H, br)	3.90 (1H, br)
13	1.70 (1H, dd, J=13.0, 12.5)	1.70 (1H, dd, J=12.9, 12.2)	1.68 (1H, m)	1.55 (1H, m)
	2.15 (1H, dd, J=13.0, 3.0)	2.15 (1H, dd, J=12.9, 2.5)	1.80 (1H, m)	1.85 (1H, m)
14	1.64 (1H, ddd, J=13.0, 12.5, 3.0)	1.64 (1H, ddd, J=13.0, 12.2, 2.5)	2.00 (1H, m)	1.97 (1H, m)
15	2.78 (1H, s)	2.79 (1H, s)	2.78 (1H, s)	2.73 (1H, s)
17	2.57 (1H, d, J=5.0)	2.58 (1H, d, J=5.1)	2.64 (1H, d, J=5.0)	2.64 (1H, d, J=5.0)
19	5.29 (1H, q, J=7.0)	5.30 (1H, q, J=7.0)	5.34 (1H, q, J=7.0)	5.30 (1H, q, J=6.5)
20	1.66 (3H, d, J=7.0)	1.67 (3H, d, J=7.0)	1.66 (3H, d, J=7.0)	1.63 (3H, d, J=6.5)
21	1.85 (3H, s)	1.84 (3H, s)	1.85 (3H, s)	1.81 (3H, s)
22	1.33 (3H, s)	1.34 (3H, s)	1.34 (3H, s)	1.39 (3H, s)
23	1.21 (3H, s)	1.22 (3H, s)	1.22 (3H, s)	1.21 (3H, s)
24	1.69 (3H, s)	1.70 (3H, s)	1.73 (3H, s)	1.69 (3H, s)
11-OMe				

No	ICM0301E(5)[b]	ICM0301F(6)[b]	ICM0301G(7)[b]	ICM0301H(8)[c]
1	1.06 (3H, t, J=7.2)	-	-	-
2	2.74 (2H, q, J=7.2)	2.31 (3H, s)	2.33(3H, s)	2.32 (3H, s)
5	7.12(1H, d, J=11.0)	7.14 (1H, d, J=11.0)	7.16 (1H, d, J=11.0)	6.98 (1H, d, J=11.0)
6	6.46 (1H, dd, J=15.0, 11.0)	6.46 (1H, dd, J=15.0, 11.0)	6.47 (1H, dd, J=15.0, 11.0)	6.38 (1H, dd, J=15.0, 11.0)
7	5.82 (1H, dd J=15.0, 10.0)	5.85 (1H, dd, J=15.0, 11.0)	5.84 (1H, dd, J=15.0, 10.5)	5.73 (1H, dd, J=15.0, 10.0)
8	2.37 (1H, m)	2.37 (1H, m)	2.35 (1H, m)	2.40 (1H, ddd, J=11.0, 10.0, 5.0)
9	1.34 (1H, m)	1.35 (1H, m)	1.70 (1H, m)	1.82 (1H, m)
10	1.06 (1H, m)	1.05 (1H,m)	1.16 (1H, m)	1.41 (1H, m)
	1.32 (1H,m)	1.34 (1H, m)	1.62 (1H, m)	1.47 (1H, m)
11	1.30 (1H, m), 1.65 (1H, m)	1.30 (1H, m), 1.65 (1H, m)	3.00 (1H, br)	3.57 (1H, br)
13	1.40 (1H, t, J=13.0)	1.42 (1H, t, J=13.0))	1.55 (1H, m)	1.65 (1H, m)
	1.79 (1H, m)	1.80 (1H, m)	1.65 (1H, m)	1.75 (1H, m)
14	1.91 (1H, m)	1.92 (1H, m)	1.90 (1H, m)	1.96 (1H, m)
15	2.77 (1H, s)	2.77 (1H, s)	2.75 (1H, s)	2.75 (1H, s)
17	2.62 (1H, d, J=5.0)	2.61 (1H, d, J=5.0)	2.63 (1H, d, J=5.0)	2.67 (1H, d, J=5.0)
19	5.31 (1H, q, J=6.5)	5.30 (1H, q, J=7.0)	5.32 (1H, q, J=7.0)	5.31 (1H, q, J=7.0)
20	1.66 (3H, d, J=6.5)	1.65 (3H, d, J=7.0)	1.66 (3H, d, J=7.0)	1.66 (3H, d, J=7.0)
21	1.84 (3H, s)	1.84 (3H, s)	1.84 (3H, s)	1.85 (3H, s)
22	1.22 (3H, s)	1.23 (3H, s)	1.23 (3H, s)	1.32 (3H, s)
23	1.22 (3H, s)	1.23 (3H, s)	1.21 (3H, s)	1.25 (3H, s)
24	1.71 (3H, s)	1.71 (3H, s)	1.70 (3H, s)	1.71 (3H, s)
11-OMe			3.27 (3H, s)	

[a] in CD_3OD at 40°C(500MHz)

[b] in CD_3OD at 24°C(400MHz)

[c] in $CDCl_3$ at 24°C(400MHz)

Table 3. ^{13}C NMR data for **1**~**8**.

carbon number	ICM0301A(1)	ICM0301B(2)	ICM0301C(3)	ICM0301D(4)	ICM0301E(5)	ICM0301F(6)	ICM0301G(7)	ICM0301H(8)
1	9.2 q	-	9.3 q	-	9.3 q	-	-	-
2	30.8 t	25.6 q	31.3 t	25.6 q	31.3 t	25.6 q	25.6 q	25.6 q
3	205.2 s	202.4 s	205.1 s	200.0 s	205.1 s	202.5 s	202.5 s	199.9 s
4	135.3 s	136.0 s	135.2 s	135.1 s	134.9 s	135.6 s	135.7 s	135.0 s
5	139.9 d	141.1 d	139.9 d	139.0 d	140.1 d	141.6 s	141.5 d	139.1 d
6	128.6 d	128.6 d	128.7 d	127.5 d	128.3 d	128.3 d	128.6 d	127.3 d
7	146.5 d	146.7 d	146.6 d	144.9 d	147.6 d	148.0 d	147.6 d	145.6 d
8	45.4 d	45.4 d	44.7 d	43.7 d	46.1 d	46.1 d	45.7 d	44.2 d
9	34.3 d	34.1 d	31.5 d	30.2 d	38.5 d	38.5 d	31.3 d	30.1 d
10	31.6 t	31.6 t	36.0 t	34.9 t	28.0 t	28.0 t	29.8 t	34.4 t
11	61.3 d	61.4 d	66.7 d	65.3 d	40.0 t	40.0 t	84.4 d	74.0 d
12	60.2 s	60.1 s	73.2 s	72.9 s	70.7 s	70.7 s	72.7 s	72.2 s
13	36.8 t	36.9 t	39.1 t	38.2 t	44.8 t	44.8 t	40.5 t	39.2 t
14	35.2 d	35.3 d	37.9 d	36.7 d	38.5 d	38.5 d	38.1 d	37.0 d
15	64.5 d	64.5 d	65.5 d	63.9 d	66.0 d	66.0 d	65.9 d	64.1 d
16	62.5 s	62.5 s	62.6 s	61.3 s	62.7 s	62.7 s	62.6 s	61.5 s
17	54.8 d	54.6 d	55.1 d	53.5 d	55.0 d	55.0 d	55.2 d	53.1 d
18	134.2 s	134.1 s	134.2 s	132.5 s	134.6 s	134.5 s	134.4 s	132.8 s
19	126.9 d	127.0 d	127.3 d	126.2 d	128.0 d	126.9 d	127.1 d	125.6 d
20	13.6 q	13.6 q	13.6 q	13.6 q	13.6 q	13.6 q	13.6 q	13.7 q
21	11.7 q	11.5 q	11.7 q	11.4 q	11.7 q	11.4 q	11.4 q	11.5 q
22	23.1 q	23.0 q	29.0 q	29.2 q	31.6 q	31.6 q	27.7 q	27.7 q
23	22.1 q	22.1 q	22.4 q	22.0 q	22.4 q	22.4 q	22.4 q	22.0 q
24	19.5 q	19.5 q	18.9 q	19.0 q	19.0 q	19.0 q	19.5 q	19.5 q
11-OMe							57.2 q	

Fig. 2a. Structure of **1** elucidated by ^1H-^1H COSY (—) and HMBC (→) experiments.

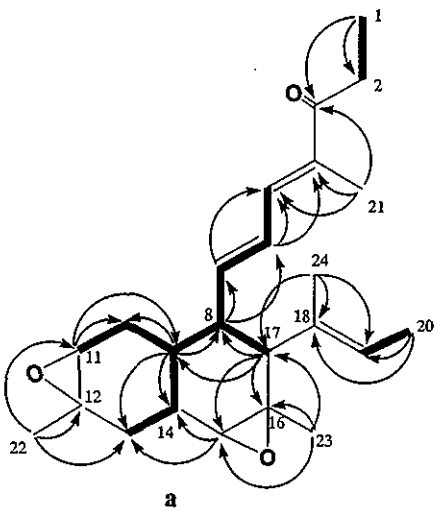

a

Fig. 2b. NOE correlations of **1**.

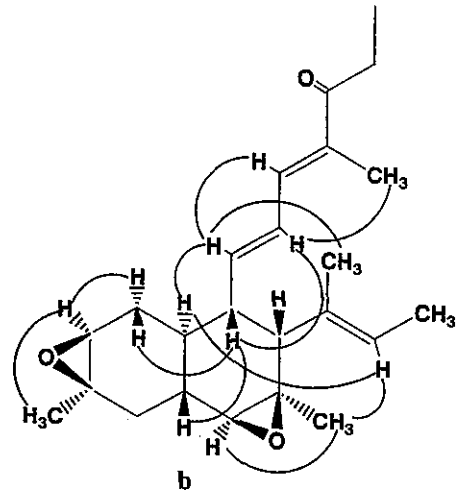

b

coupling constant (J=13.0 Hz) due to the diaxial relationship between H-9 and H-14 indicated a *trans* junction for the decalin ring. The vicinal coupling constants between H-9 and H-8 (J=11.0 Hz) also indicated the diaxial relationship, whereas coupling constant between H-8 and H-17 (J=5.0 Hz) indicated an *axial-equatorial* relationship. The observation of an NOE between H-8 and the two protons H-10_{ax} and H-14 indicate the 1,3-diaxial relationship between H-8 and H-14 and the trans nature of the ring junction. An NOE was observed between H-11 and methyl protons (H-22), and between H-15 and methyl protons (H-23), respectively. On the other hand, no coupling was observed between H-11 and H-10_{ax} and between H-14 and H-15 perhaps due to the dihedral angles of near 90°. These results indicated that the two methyl protons (H-22 and H-23) exist on the α side of the decalin ring system. Accordingly, two epoxy moieties should exist on the β side of the decalin ring as shown in Fig. 2b. The geometry of the diene system was established to be 4*E*, and 6*E* based on the coupling constant ($J_{6,7}$=15.0 Hz) and the NOE observation between methyl protons (H-21) and H-6. The geometry of double bond at C-18 was elucidated as follow. NOE was observed between methyl protons (H-24) and an olefinic proton (H-7). On the other hand, NOE was observed between H-19 and H-23, H-9. Therefore, H-19 occupied near space to H-9 and methyl protons (H-23). Subsequently, two methyls (H-24 and H-20) should be located on the opposite side of H-19. These results are indicative of 18E configuration as shown in Fig. 2b. The structure of **1** was structurally related to fusarielin[6].

Structure of ICM0301 B (2)

The molecular formula of ICM0301B (**2**) was determined to be $C_{23}H_{32}O_3$ on the basis of the HRESI-MS and ^{13}C NMR information indicating the lack of one carbon and two hydrogen atoms compared with that of **1**. The UV and IR spectra were almost the same as **1**. The ^{13}C NMR spectra of **1** and **2** were also similar to each other except for the disappearance of signal due to one methylene carbon in **2**. In the ^1H NMR spectrum of **2**, acetyl protons were observed at δ_H 2.31 (s, 3H). These results indicated that a propionyl group of **1** was replaced by an acetyl group in **2**. Detailed NMR spectral analyses including ^1H-^1H COSY and HMBC experiments elucidated the planar structure of **2** as shown in Fig. 1. NOESY and NOE difference spectra of **2** showed that the relative stereochemistry of **2** was identical with that of **1**. Thus it was concluded that the structure of **2** was shown in Fig. 1.

The structures of other minor components were subsequently determined by comparing their spectral data with those of **1** and **2**.

Structure of ICM0301 C (3)

The molecular formula of ICM0301C (**3**) was determined to be $C_{24}H_{35}O_3Cl$ by HRESI-MS and ^{13}C NMR spectra together with the characteristic mass fragment patterns of chlorine containing molecules. The ^1H and ^{13}C NMR spectra of **3** showed a close similarity to those of **1** except for the H-11, C-10, C-11, C-12 and C-22 chemical shifts (Table 2). The ^1H-^1H COSY and HMBC spectra of **3** indicated the presence of the same carbon skeleton as that of **1**. Although one oxirane ring was preserved in **3** based on the large coupling constant ($^1J_{C\text{-}15,H\text{-}15}$=175 Hz), the other one might be cleaved based on the coupling constant ($^1J_{C\text{-}11,H\text{-}11}$=152 Hz). This value strongly supported the presence of chloromethine[7] in the molecule. In addition, the observation that the quaternary carbon (C-12, δ_C 60.2) in **1** was shifted to low field (δ_C 73.2) due to the presence of the hydroxymethine in **3** was consistent with this conclusion. The remaining parts of **3** showed a close similarity to **1** in the NMR spectroscopic properties including ^1H-^1H COSY, HMBC, NOESY spectra. Therefore, the structure of **3** was proposed as shown in Fig. 1.

Structure of ICM0301 D (4)

ICM0301D (**4**) was obtained as a white powder. Most of the spectroscopic properties of **4** were similar to those of **3**. The molecular formula of **4** was determined to be $C_{23}H_{33}O_3Cl$ on the basis of the HRESI-MS, suggesting that **4** was one methylene unit lower than that of **3**. The ^1H and ^{13}C NMR spectra of **3** and **4** were similar to each other except for the terminal parts of long side chains. Consequently, the structure of **4** was determined as shown in Fig. 1.

Structure of ICM0301 E (5)

The molecular formula of ICM0301E (**5**) was determined to be $C_{24}H_{36}O_3$. Compound **5** contained four methylene carbons based on the observation of DEPT experiments. Among them, three methylene carbons (C-2, C-10, C-13) in **5** were identical with those of **3** on the basis of NMR analyses. On the other hand, one more methylene (C-11), which was readily identified by the correlation between H-10 protons in ^1H-^1H COSY, was observed in the DEPT spectrum of **5**. The remaining parts of **5** were

identical with those of **3**. These results indicated that the methylene (C-11) in **3** was replaced by chloromethine in **5**. Thus, the structure of **5** was determined as shown in Fig. 1.

Structure of ICM0301 F (**6**)

The molecular formula ($C_{23}H_{34}O_3$) of ICM0301F (**6**) and most of the spectroscopic properties were very similar to those of **5**. Just as is the case for compound **2** and **4**, the difference between **6** and **5** exists in the terminal of long side chains as shown in Fig. 1.

Structure of ICM0301 G (**7**)

The molecular formula of ICM0301G (**7**) was determined to be $C_{24}H_{36}O_4$ on the basis of HRESI-MS and the ^{13}C NMR. In the ^1H NMR spectrum of **7**, characteristic methoxy protons at δ_H 3.27 were observed, in distinction with signals seen in the spectra of compounds **1**~**6**. The methyl protons correlated to C-11 methine carbon (δ_C 84.4) in the HMBC spectrum indicating the presence of methoxymethine at C-11. The remaining parts of **7** were identical with those of **4** and **6**. Thus, the structure of **7** was determined as shown in Fig. 1.

Structure of ICM0301 H (**8**)

The molecular formula of ICM0301H (**8**) was determined to be $C_{23}H_{34}O_4$ on the basis of HRESI-MS, which is one carbon and two protons less than that of **7**. In the ^1H NMR spectrum of **8**, a methoxy group was not observed. In the ^{13}C NMR spectrum, a low-field methine carbon (C-11, δ_C 84.4) in **7** was shifted to high-field (δ_C 74.0) in **8**. These results indicated that a methoxy group in **7** was replaced by a hydroxyl group in **8** as shown in Fig. 1.

As described above, ICM0301s were isolated as new angiogenesis inhibitors. Among them, ICM0301A and B were produced as major products. On the other hand, minor compounds (**3**~**8**) were isolated from larger scale fermentations. Taking the chemical reactivity of epoxy functional group into consideration, some of minor components might be artifacts of the isolation procedures.

Materials and Methods

UV spectra were measured on a Hitachi 228A spectrometer. IR spectra were recorded on a Horiba FT-200 fourier transform infrared spectrometer. Optical rotations were measured with a Perkin-Elmer 241 polarimeter. HRESI-MS spectra were measured with a JEOL JMS-T100LC. HRFAB-MS spectra were measured with a VG AutoSpec mass spectrometer. The ^1H and ^{13}C NMR spectra of **1** and **2** were measured on a JEOL JNM-A500 spectrometer at 40°C using TMS as an internal reference. Compounds **3**~**8** were measured on a JEOL JNM-A400 spectrometer at 24°C.

Acknowledgment

We are grateful to Dr. RYUICHI SAWA of Microbial Chemistry Research Center for the measurement of HRESI-MS spectra. This work was supported in part by a Grant-in-Aid for Scientific Research from the Ministry of Education, Science, Sports and Culture in Japan.

References

1) OTUKA, T.; T. SHIBATA, Y. TSURUMI, S. TAKASE, M. OKUHARA, H. TERANO, M. KOHSAKA & H. IMANAKA: A new angiogenesis inhibitor, FR-111142. J. Antibiotics 45: 348~354, 1992
2) YANASE, T.; M. TAMURA, K. FUJITA, S. KODAMA & K. TANAKA: Inhibitory effect of angiogenesis inhibitor TNP-470 on tumor growth and metastasis of human cell lines *in vitro* and *in vivo*. Cancer Res. 53: 2566~2570, 1993
3) SIN, N.; L. MENG, M. Q. WANG, J. J. WEN, W. G. BORNMANN & C. M. CREWS: The anti-angiogenetic agent fumagillin covalently binds and inhibits the methionine aminopeptidase, MetAP-2. Pro. Natl. Acad. Sci. 94: 6099~6103, 1997
4) KUMAGAI, H.; T. SOMENO, K. DOBASHI, K. ISSHIKI, M. ISHIZUKA & D. IKEDA: ICM0301s, new angiogenesis inhibitors from *Aspergillus* sp. F-1491. I. Taxonomy, fermentation, isolation and biological activities. J. Antibiotics 57: 97~103, 2004
5) BREITMAIER, E. & W. VOELTER: "Carbon-13 NMR Spectroscopy, Methods and Applications". Verlag-Chemie, Bergstr., 1974
6) KOBAYASHI, H.; R. SUNAGA, K. FURIHATA, N. MORISAKI & S. IWASAKI: Isolation and structure of an antifungal antibiotic, fusarielin A, and related compounds produced by *Fusarium* sp. J. Antibiotics 48: 42~52, 1995
7) PRETSCH, E. (*Ed.*): Tabellen zur Strukturaufklärung Organischer Verbindungen mit Spektroskopischen Methoden. Springer-Verlag, Berlin Heidelberg, 1976

Available online at www.sciencedirect.com
SCIENCE DIRECT®
Bioorganic & Medicinal Chemistry Letters
ELSEVIER
Bioorganic & Medicinal Chemistry Letters 15 (2005) 1867–1871

Structure-based design of derivatives of tyropeptin A as the potent and selective inhibitors of mammalian 20S proteasome

Isao Momose,[a,*] Yoji Umezawa,[b] Sehei Hirosawa,[c] Hironobu Iinuma[b] and Daishiro Ikeda[a]

[a]*Numazu Bio-Medical Research Institute, Microbial Chemistry Research Center, 18-24 Miyamoto, Numazu City, Shizuoka 410-0301, Japan*
[b]*Microbial Chemistry Research Center, 3-14-23 Kamiosaki, Shinagawa-ku, Tokyo 141-0021, Japan*
[c]*Hiyoshi Medicinal Chemistry Research Institute, Microbial Chemistry Research Center, 3-34-17 Ida, Nakahara-ku, Kawasaki-shi, Kanagawa, 211-0035, Japan*

Received 12 January 2005; revised 3 February 2005; accepted 4 February 2005

Abstract—Tyropeptin A, a new potent proteasome inhibitor, was produced by *Kitasatospora* sp. MK993-dF2. To enhance the inhibitory potency of tyropeptin A, we constructed the structural model of tyropeptin A bound to the site responsible for the chymotrypsin-like activity of mammalian 20S proteasome. Based on these modeling experiments, we designed and synthesized several derivatives of tyropeptin A. Among them, the most potent compound, TP-104, exhibited a 20-fold enhancement in its inhibitory potency compared to tyropeptin A. Additionally, TP-110 specifically inhibited the chymotrypsin-like activity, but did not inhibit the PGPH and the trypsin-like activities.

1. Introduction

The 26S proteasome consists of a central catalytic 20S proteasome and two terminal regulatory complexes, termed PA700 (also known as the 19S regulatory complex), which are attached to both ends of the central portion.[1,2] The 20S proteasome is a large cylindrically-shaped complex composed of two copies each of seven distinct α- and seven distinct β-type subunits. All the subunits of yeast 20S proteasome have been cloned and sequenced, and can be grouped by sequence homology.[3] The 20S proteasome possesses at least three distinctive protease activities of the post-glutamyl-peptide hydrolyzing (PGPH), trypsin-like and chymotrypsin-like activities, and were assigned to the active subunits of β1, β2, and β5, respectively.

Proteasome degrades numerous regulatory proteins, such as cyclins, cyclin-dependent kinase inhibitors (e.g., p21 and p27), tumor suppressors (e.g., p53), and the inhibitory proteins of the NF-κB activation (e.g., IκB-α), which are critical in tumor growth.[4–7] Proteasome inhibitors can stabilize these regulatory proteins, and cause cell cycle arrest and apoptosis, and, as a result, can limit the tumor development. In 2003, PS-341, a dipeptide boronic acid proteasome inhibitor,[8–10] was approved for cancer treatment for multiple myeloma patients. Therefore, the proteasome inhibitor is useful for the treatment of cancer.

Previously, we described the isolation and characterization of a new proteasome inhibitor, tyropeptin A, which was produced by *Kitasatospora* sp. MK993-dF2.[11–13] The structure of tyropeptin A is isovaleryl-L-tyrosyl-L-valyl-DL-tyrosinal. Tyropeptin A significantly inhibits chymotrypsin-like activity in the three distinct protease activities of the 26S proteasome.

In the present study, to enhance the inhibitory potency of tyropeptin A, we constructed a structural model of tyropeptin A bound to the site responsible for the chymotrypsin-like activity of the mammalian 20S proteasome. We now report the utilization of the constructed model for the design of reasonable and effective modifications of tyropeptin A.

Keyword: Proteasome inhibitor.
* Corresponding author. Tel.: +81 55 924 0601; fax: +81 55 922 6888; e-mail: imomose@bikaken.or.jp

0960-894X/$ - see front matter © 2005 Elsevier Ltd. All rights reserved.
doi:10.1016/j.bmcl.2005.02.013

2. Model of tyropeptin A bound to the β5/β6 site of mammalian 20S proteasome

The crystal structure of the yeast 20S proteasome with a bound peptide aldehyde inhibitor, acetyl-L-leucyl-L-leucyl-L-norleucinal, revealed that the binding site responsible for the chymotrypsin-like activity of the 20S proteasome is formed by the association of the β5 and β6 subunits.[14] Therefore, it is reasonable to conclude that the binding site responsible for the chymotrypsin-like activity of the mammalian 20S proteasome will also be formed by the association of the β5 and β6 subunits. Though the crystal structure of the human 20S proteasome has not yet been determined, the crystal structure of the mammalian 20S proteasome isolated from bovine was recently determined.[15,16] The crystal structures and the amino acid sequences of the α2, β1, β5, β6, and β7 subunits of the bovine 20S proteasome are different from the *S. cerevisiae* 20S proteasome. Since the amino acid sequences of the β5 and β6 subunits of the bovine 20S proteasome show a 100% identity to those of the human 20S proteasome, the structural model of the β5/β6 site in the bovine proteasome adequately represents the β5/β6 site of the human proteasome. One possible binding model of tyropeptin A to the β5/β6 site of the mammalian 20S proteasome is shown in Figure 1.[17] Figure 1A shows the expected binding mode of tyropeptin A to the β5/β6 site. It is conceivable that the aldehyde group of tyropeptin A forms a hemiacetal adduct with the catalytic Thr 1 residue of the β5 subunit. Therefore, it is assumed that the tyrosinal, valine, and tyrosine residues of tyropeptin A mimic the role of the P1, P2, and P3 amino acids of the binding sites[18] in the natural substrate of the proteasome, respectively. In addition, it is thought that residues Thr 21, Gly 47, and Ala 49 in the β5 subunit and Asp 125 in the β6 subunit are involved in the recognition of the peptide bonds of the substrate. Hence, assuming that tyropeptin A forms five β-sheet-like hydrogen bonds with the four residues, Thr 21, Gly 47, Ala 49, and Asp 125, and a hemiacetal adduct with the catalytic Thr 1 residue, we investigated the most favorable orientation of tyropeptin A in the β5/β6 binding site model using these hydrogen bonds and the adduct as modeling constraints. As a result, tyropeptin A nicely fits into the β5/β6 site (Fig. 1B). Figure 1B is an overview of the binding model of tyropeptin A bound to the β5/β6 site. Tyropeptin A was encircled by the association of the β5 and β6 subunits. In this binding model, four CH/π interactions were observed (Fig. 1A). The CH/π interaction is a hydrogen-bond-like weak attractive force observed between a CH hydrogen and π electron system, which was recently revealed to have a critical role in protein–ligand complexation and protein folding.[19] The CH hydrogens of the side chains of Val 31, Lys 33, and Ala 49 in the β5 subunit were able to form the CH/π interactions with the π electron systems of the tyrosinal residue in tyropeptin A at the P1 position. The CH hydrogen of Ala 20 in the β5 subunit was able to form the CH/π interaction with the π electron systems of the tyrosine residue in tyropeptin A at the P3 position. In contrast, hydrogen bonds and/or CH/π interactions between the *N*-terminal isovaleryl

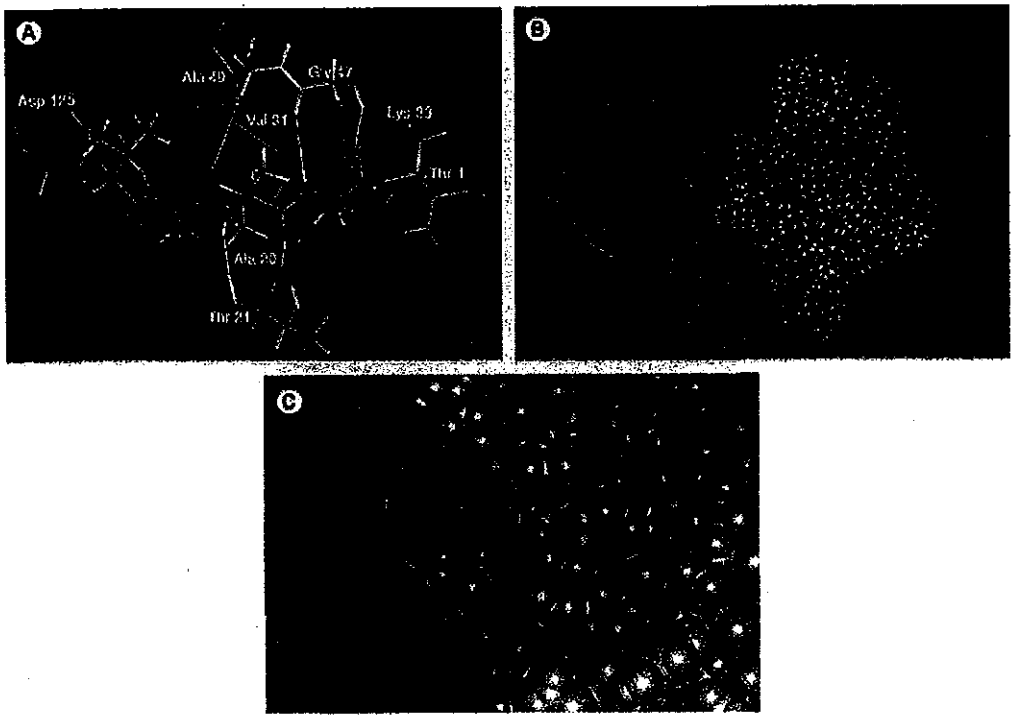

Figure 1. Binding model of tyropeptin A bound to the site responsible for the chymotrypsin-like activity of the 20S proteasome. (A) Expected binding mode of tyropeptin A to β5/β6 site. Tyropeptin A, atom colors; hydrogen bond, sky blue; CH/π interaction, red; β5/β6 site, gray. (B) Overview of binding model of tyropeptin A bound to the β5/β6 site of the 20S proteasome. Subunit β5, gray; subunit β6, green; tyropeptin A, yellow. (C) Binding model of tyropeptin A in the β5/β6 site. Subunit β5, gray; subunit β6, green; tyropeptin A, yellow.

moiety of tyropeptin A and the 20S proteasome were not observed. This binding model suggested the presence of an open space in the vicinity of the *N*-terminal of tyropeptin A (Fig. 1C, sky blue circle). Since the isovaleryl moiety in tyropeptin A only partially filled this area, we speculated that a compound capable of filling the open space may exhibit the enhanced inhibitory activity against the chymotrypsin-like activity of the 20S proteasome. Therefore, we designed tyropeptin A derivatives having a bulky *N*-terminal moiety.

3. Derivatives of tyropeptin A

According to the modeling studies mentioned above, we synthesized tyropeptin A derivatives modified at the *N*-terminal moiety and evaluated their inhibitory activities of 20S proteasome as shown in Table 1.[20] TP-104 exhibited a 20-fold inhibitory potency enhancement for the chymotrypsin-like activity compared to tyropeptin A. This increase in the inhibitory potency of TP-104 may come from the formation of hydrophobic or CH/π interactions between the 1-naphthyl moiety and the β5/β6 site. To prove this hypothesis, we constructed a structural model of TP-104 bound to the β5/β6 site of the 20S proteasome (Fig. 2). Figure 2A shows the comparison with the three-dimensional structures of tyropeptin A and TP-104 at the β5/β6 site. As shown in Figure 2A, the 1-naphthyl moiety of TP-104 (right) well complements the shape of the open space in the vicinity of the *N*-terminal of tyropeptin A (left). Figure 2B shows the expected binding mode of TP-104 to the β5/β6 site. As expected, new interactions between the 1-naphthyl moiety and the β5/β6 site were observed. The CH hydrogens of the side chain of Ala 50 in the β5 subunit and Val 127 in the β6 subunit were able to form CH/π interactions with the 1-naphthyl moiety of TP-104. Since new CH/π interactions between the 1-naphthyl moiety of TP-104 and the β5/β6 site were formed, TP-104 had a very high affinity for the β5/β6 site. Therefore, TP-104 might be expected to show an increased inhibitory activity for the chymotrypsin-like activity of the 20S proteasome relative to tyropeptin A, which agrees with our experimental results.

The di-*O*-methyl derivative of TP-104, TP-110, inhibits the chymotrypsin-like activity with an IC_{50} value of 0.027 μM, but shows a marked decrease in its inhibitory activity for the trypsin-like activity (Table 1). TP-110 did not inhibit the trypsin-like and the PGPH activities even at the concentration of 100 μM, leading to an enhanced specificity for the chymotrypsin-like activity. The binding site of the trypsin-like activity is formed by the association of the β2 and the β3 subunits.[16] The S1 and S3 pockets of the β2/β3 site were narrower than those of the β5/β6 site. Hence, the di-*O*-methyl derivative of TP-104, TP-110, may not optimally fit into the β2/β3 site. Therefore, TP-110 is a potent and selective inhibitor for the chymotrypsin-like activity of the mammalian 20S proteasome.

Our modeling studies of tyropeptin A bound to the 20S proteasome successfully designed the two compounds, TP-104 having a highly potent inhibitory activity against the 20S proteasome activities, and also TP-110, which specifically inhibits the chymotrypsin-like activity of the 20S proteasome. In this manner, our binding model of the bovine proteasome allowed us to rationally design potent inhibitors for the 20S proteasome. The evaluation of the anticancer activity of these compounds will be reported elsewhere.

Table 1. Inhibitory activities of the 20S proteasome by tyropeptin A derivatives

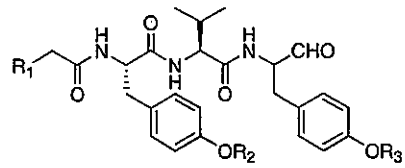

Compound	R_1	R_2	R_3	IC_{50} (μM)		
				Chymotrypsin-like activity	PGPH activity	Trypsin-like activity
Tyropeptin A	$CH(CH_3)_2$	H	H	0.14	68	5
TP-101	C_6H_{11}	H	H	0.033	17	3
TP-102	C_6H_5	H	H	0.027	16	2
TP-103	2-Naphthyl	H	H	0.014	4.7	0.7
TP-104	1-Naphthyl	H	H	0.007	4.9	1.2
TP-105	$CH_2(CH_2)_3CH_3$	H	H	0.037	20	2
TP-106	$CH(CH_3)_2$	H	CH_3	0.19	21	21
TP-107	$CH(CH_3)_2$	CH_3	CH_3	0.12	56	37
TP-108	1-Naphthyl	H	CH_3	0.018	38	6
TP-109	1-Naphthyl	CH_3	H	0.020	31	6
TP-110	1-Naphthyl	CH_3	CH_3	0.027	>100	>100
TP-111	$N(CH_3)_2$	H	H	1.2	>100	7.8
MG132				0.068	1.4	4.5

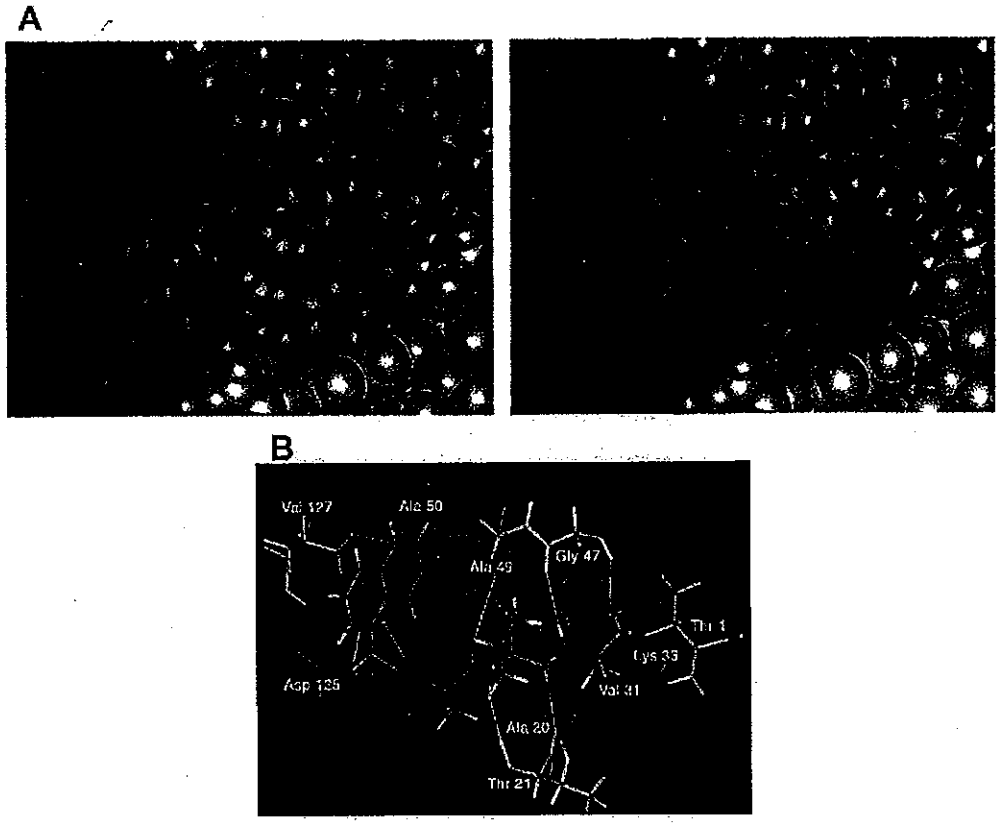

Figure 2. Binding model of TP-104 bound to the β5/β6 site of the 20S proteasome. (A) Comparison with structures of tyropeptin A and TP-104 in the β5/β6 site. Binding model of TP-104 in the β5/β6 site (right) compared to the tyropeptin A (left). Tyropeptin A is yellow and TP-104 is violet. (B) Expected binding mode of TP-104 to the β5/β6 site. Tyropeptin A atom colors; hydrogen bond, sky blue; CH/π interaction, red; β5/β6, gray.

Acknowledgements

We would like to thank Dr. R. Sawa and Ms. Y. Kubota, Microbial Chemistry Research Center, for spectroscopic analysis, and Dr. T. Watanabe and Mr. M. Abe, Microbial Chemistry Research Institute, for useful discussions. This work was supported by the Public Trust Haraguchi Memorial Cancer Research Fund and a Grant-in-Aid for Scientific Research from the Japanese Ministry of Education, Culture, Sports, Science, and Technology (No 15790059).

References and notes

1. Coux, O.; Tanaka, K.; Goldberg, A. L. *Annu. Rev. Biochem.* **1996**, *65*, 801.
2. Voges, D.; Zwickl, P.; Baumeister, W. *Annu. Rev. Biochem.* **1999**, *68*, 1015.
3. Heinemeyer, W.; Tröndle, N.; Albrecht, G.; Wolf, D. H. *Biochemistry* **1994**, *33*, 12229.
4. Maki, C. G.; Howley, P. N. *Mol. Cell Biol.* **1997**, *17*, 355.
5. Pagano, M.; Tam, S. W.; Theodoras, A. M.; Beer-Romero, P.; Del Sal, G.; Chau, V.; Yew, P. R.; Draetta, G. F.; Rolfe, M. *Science* **1995**, *269*, 682.
6. Ciechanover, A.; DiGiuseppe, J. A.; Bercovich, B.; Orian, A.; Richter, J. D.; Schwartz, A. L.; Brodeur, G. M. *Proc. Natl. Acad. Sci. U.S.A.* **1991**, *88*, 139.
7. Palombella, V. J.; Rando, O. J.; Goldberg, A. L.; Maniatis, T. *Cell* **1994**, *78*, 773.
8. Adams, J.; Behnke, M.; Chen, S.; Cruickshank, A. A.; Dick, L. R.; Grenier, L.; Klunder, J. M.; Ma, Y.-T.; Plamonda, L.; Stein, R. L. *Bioorg. Med. Chem. Lett.* **1998**, *8*, 333.
9. Adams, J.; Palombella, V. J.; Sausville, E. A.; Johnson, J.; Destree, A.; Lazarus, D. D.; Maas, J.; Pien, C. S.; Prakash, S.; Elliott, P. *J. Cancer Res.* **1999**, *59*, 2615.
10. Richardson, P. G.; Barlogie, B.; Berenson, J.; Singhal, S.; Jagannath, S.; Irwin, D.; Rajkumar, S. V.; Srkalovic, G.; Alsina, M.; Alexanian, R.; Siegel, D.; Orlowski, R. Z.; Kuter, D.; Limentani, S. A.; Lee, S.; Hideshima, T.; Esseltine, D. L.; Kauffman, M.; Adams, J.; Schenkein, D. P.; Anderson, K. C. *New Engl. J. Med.* **2003**, *348*, 2609.
11. Momose, I.; Sekizawa, R.; Hashizume, H.; Kinoshita, N.; Homma, Y.; Hamada, M.; Iinuma, H.; Takeuchi, T. *J. Antibiot.* **2001**, *54*, 997.
12. Momose, I.; Sekizawa, R.; Hirosawa, S.; Ikeda, D.; Naganawa, H.; Iinuma, H.; Takeuchi, T. *J. Antibiot.* **2001**, *54*, 1004.
13. Momose, I.; Sekizawa, R.; Iinuma, H.; Takeuchi, T. *Biosci. Biotechnol. Biochem.* **2002**, *54*, 1004.
14. Groll, M.; Ditzel, L.; Löwe, J.; Stock, D.; Bochtler, M.; Bartunik, H. D.; Huber, R. *Nature* **1997**, *386*, 463.
15. Unno, M.; Mizushima, T.; Morimoto, Y.; Tomisugi, Y.; Tanaka, K.; Yasuoka, N.; Tsukihara, T. *J. Biochem. (Tokyo)* **2002**, *131*, 171.
16. Unno, M.; Mizushima, T.; Morimoto, Y.; Tomisugi, Y.; Tanaka, K.; Yasuoka, N.; Tsukihara, T. *Structure* **2002**, *10*, 609.

17. X-ray crystal structure data of the bovine 20S proteasome were taken from the Protein Data Bank with the accession code 1IRU. The complex model structure was optimized with the Discover program of Insight II (Accelrys). The CH/π interactions were detected by the CHPI program (Nishio, M.; Hirota, M.; Umezawa, Y. *The CH/π Interaction. Evidence, Nature, and Consequences*; Wiley-VCH: New York, 1998). This program was written in order to search for the short contacts between the CH groups and π system in protein structures, and is able to detect XH/π interactions (X = C, N, O, and S) based on bond length and angle parameters.
18. Schechter, I.; Berger, A. *Biochem. Biophys. Res. Commun.* **1967**, *27*, 157.
19. Umezawa, Y.; Nishio, M. *Bioorg. Med. Chem.* **1998**, *6*, 493.
20. The chymotrypsin-like, trypsin-like and PGPH activities of the 20S proteasome were measured using fluorogenic substrates as previously described.[11] 20S proteasome was prepared from human leukemia HL-60 cells.

J. Antibiot. 58(1): 56–60, 2005

ORIGINAL ARTICLE

THE JOURNAL OF ANTIBIOTICS

Absolute Configuration of Kigamicins A, C and D

Tetsuya Someno, Setsuko Kunimoto, Hikaru Nakamura, Hiroshi Naganawa, Daishiro Ikeda

Received: October 22, 2004 / Accepted: December 7, 2004

Abstract The stereochemistry of kigamicins A (**1**), C (**2**) and D (**3**) were elucidated by a combination of X-ray crystallographic analysis and degradation studies. The absolute structures of kigamicins thus determined were depicted as shown in Fig. 2.

Keywords kigamicin, natural products, antitumor antibiotics, absolute configuratioin, X-ray crystallography

Introduction

In the course of screening for new antitumor antibiotics, we have isolated five new antibiotics, kigamicins [1, 2], from the culture broth of *Amycolatopsis* sp. ML630-mF1 by their selective killing activities against PANC-1 cells only under a nutrient starvation condition. Among them, kigamicin D, the major compound in the cultured broth showed antitumor activities [1, 3] *in vitro* and *in vivo*. Kigamicins also showed antimicrobial activities against Gram-positive bacteria including methicillin-resistant *Staphylococcus aureus* (MRSA). The planar structures of kigamicins were elucidated by NMR and MS spectral analyses [2]. The structures of kigamicins were found to be composed of an aglycon of fused octacyclic ring and deoxy sugars. However, the relative and absolute configuration of kigamicins has not been determined based on the NMR studies alone due to the lack of NOE information. In this paper, we describe the absolute structures of kigamicins A, C and D determined by NMR analysis, chemical degradation studies and X-ray crystallographic analyses.

Results and Discussion

Determination of stereochemistry was conducted at first for kigamicin A (**1**), because other members of the antibiotics could not be crystallized in all solvents so far used. Compound **1** was crystallized from hot MeOH/H_2O to give yellow plate crystals. The relative stereochemistry of **1** was thus determined by X-ray analysis as shown in Fig. 1.

In order to determine the absolute structure of **1**, the configuration of amicetose was examined by measuring its optical rotation value after hydrolysis of **1** as shown in Scheme 1. Treatment of **1** with 1 N HCl in THF at room temperature for 18 hours gave an aglycon (**4**) in 76% yield and amicetose (**5**) in 90% yield. The aglycon part was proved to be identical with those derived from the other kigamicins in all spectroscopic properties. The optical rotation value of **5** was $[\alpha]_D^{22}$ +42.5° (*c* 0.7, Me_2CO), which is identical to the reported value of D-amicetose; $[\alpha]_D^{22}$ +43.6° (*c* 1.0, Me_2CO) [4, 5]. Therefore, amicetose (**5**) in **1** was determined to be D-form. Taking the configuration of amicetose into consideration, the absolute stereochemistry of **1** was determined as shown in Fig. 2 having 12*S*, 14*R*, 15*S*, 20*R*, 26*R* configurations as an aglycon. In addition, the coupling constant of anomeric proton (J=2.0, 9.0 Hz) [2] in **1** indicated the presence of β-

T. Someno (Corresponding author), **S. Kunimoto, D. Ikeda:** Numazu Bio-Medical Research Institute, Microbial Chemistry Research Center, 18-24 Miyamoto, Numazu-shi, Shizuoka 410-0301, Japan, E-mail: numazu@bikaken.or.jp

H. Nakamura, H. Naganawa: Microbial Chemistry Research Center, 3-14-23 Kamiosaki, Shinagawa-ku, Tokyo 141-0021, Japan

D amicetoside, which is consistent with the results obtained by X-ray analysis.

As reported in a previous paper [2], kigamicin D contained one amicetose and two oleandrose moieties. Since there are discrepancies between the reported optical rotation values of oleandrose [6~8], and since the complete separation of amicetose and oleandrose in the hydrolysate of kigamicin D was difficult, we attempted to obtain di- or tri-saccharides containing amicetose and oleandrose as crystals. As shown in Scheme 2, mild acid hydrolysis of **3** yielded amicetose, oleandrose, disaccharide (**6**) and trisaccharide (**7**) as well as aglycon (**4**), kigamicin A (**1**) and kigamicin C (**2**). This result indicated that the absolute configurations of aglycon and amicetose moieties in **1**, **2** and **3** were identical. Compounds **6** and **7** were crystallized from EtOAc/*n*-hexane and ether/*n*-hexane to give colorless crystals with melting point of 133~136°C and 161~163°C, respectively. The X-ray structural analysis of **7** exhibited the presence of anomeric mixture (α-anomer : β-anomer=55 : 45). Fig. 3 shows the ORTEP drawing of **7** (α-anomer) by a single crystal X-ray analysis. Since the absolute configuration of amicetose had been determined to be D, two oleandrose moieties were established to be both D-forms. On the basis of the above observation, the absolute structure of kigamicin D (**3**) was depicted as shown in Fig. 2 having 12*S*, 14*R*, 15*S*, 20*R*, 26*R* configurations as an aglycon and D-amicetose and D-oleandrose as deoxy sugar moieties. Coincidentally, the

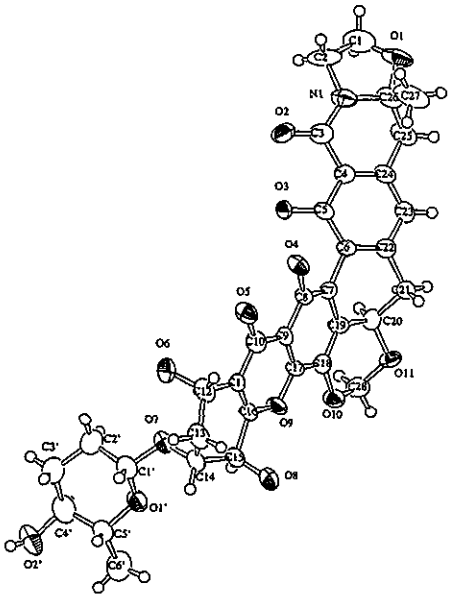

Fig. 1 X-ray crystal structure of kigamicin A.

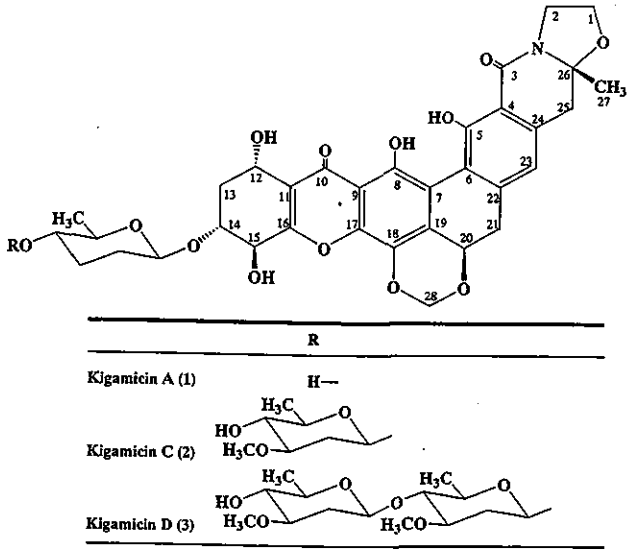

Fig. 2 Structures of kigamicins A (**1**), C (**2**) and D (**3**).

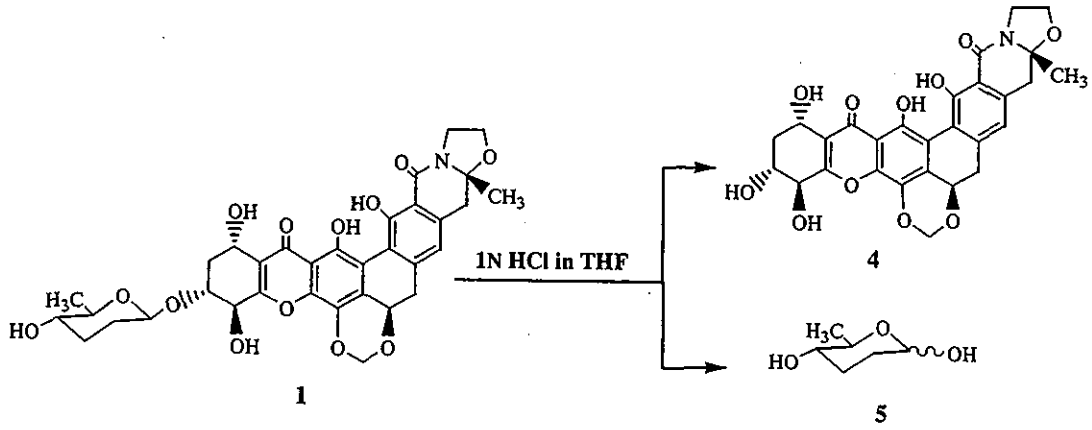

Scheme 1

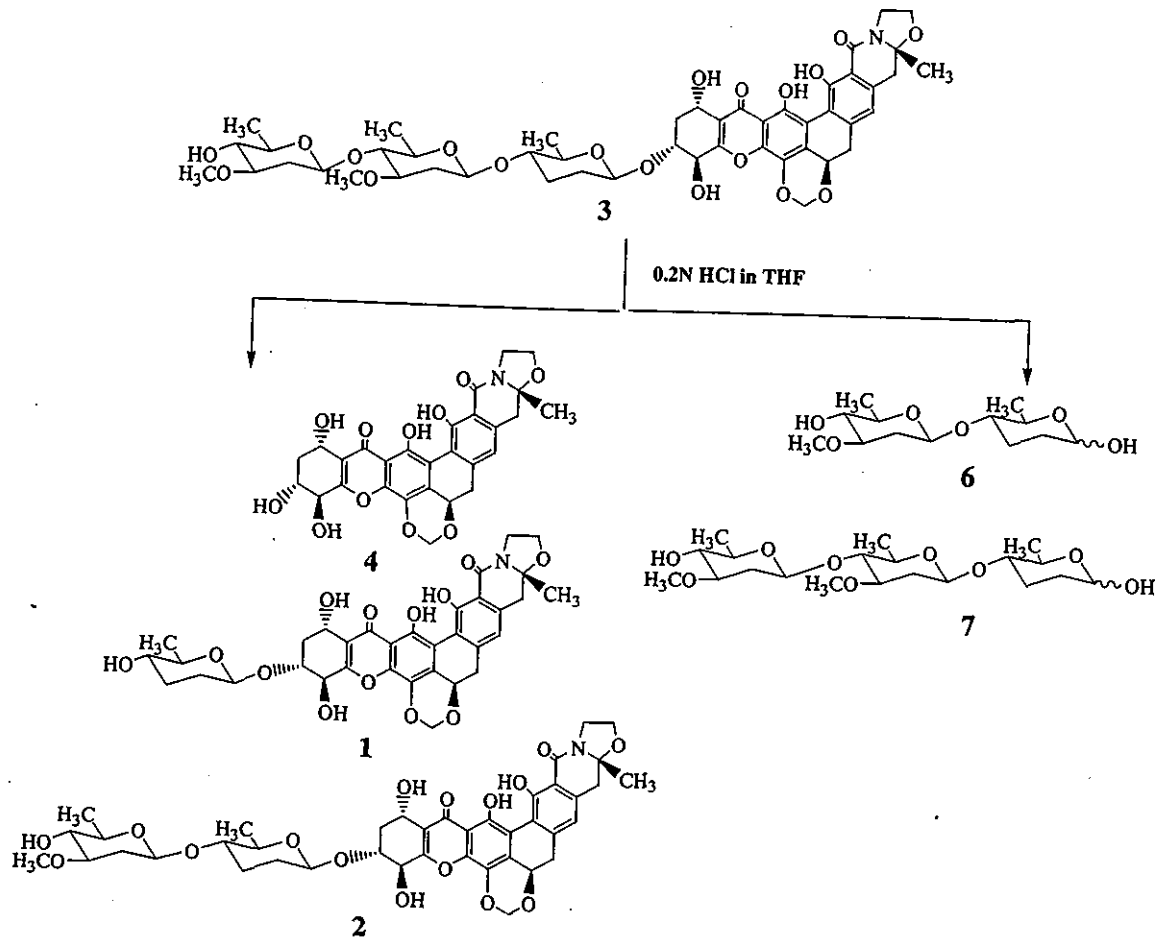

Scheme 2

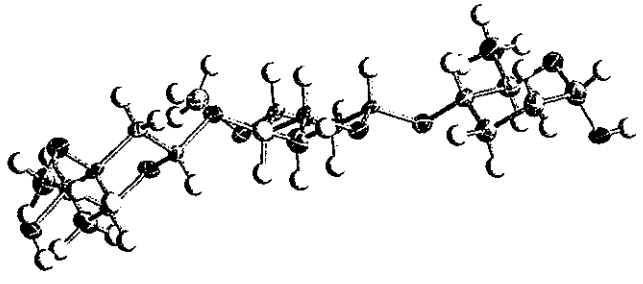

Fig. 3 X-ray crystal structure of trisaccharide (**7**).

absolute structure of kigamicin C (**2**) could be determined as shown in Fig. 2.

As described in this paper, the absolute structures of kigamicins A, C and D were determined. The structures of kigamicins are unique in that mono-, di-, tri- and tetrasaccharide moieties are attached to the polycyclic xanthone moiety. Other members of this family include cervinomycin [9], actinoplanones [10], LL-E19085α [11], LL-D42067 [12], BE-13793X [13], MS 901809 [14] and FD-594 [15]. Among them, MS 901809, FD-594 and BE-13793X were glycosides. Kondo *et al.* [15] reported an attractive biosynthetic pathway of FD-594 and MS901809, in which the glycosidic position of both compounds are C-13 and C-15, respectively. They postulated that the same benzo[*a*]naphthacenequinone chromophore may be derived at an early stage. Then, Baeyer-Villiger type oxidation occurs at a quinone carbonyl group. After the production of ring-opened intermediate, recyclization via different hydroxyl group results in two structurally related compounds. Kigamicins may be biosynthesized in the same manner. However, it is noteworthy from the viewpoint of biosynthesis that the glycosidic position of kigamicins is C-14 instead of C-15 and C-13. Although the limited supply of kigamicin B and E prevented the determination of their stereochemistry, the absolute configuration of both compounds may be identical with kigamicin D due to the kigamicin biosynthesis.

Up to now, there are few X-ray crystallographic data on

polycyclic xanthones due to the difficulty in obtaining suitable single crystals for X-ray analysis [9] and there are very few polycyclic xanthones whose absolute structures have been determined. Fortunately, we could obtain single crystals of **1** and using them could successfully carry out the absolute structure determination of kigamicins.

Further biological evaluation of kigamicins is in progress.

Experimental

General

Melting points were determined with a Yanagimoto micro melting point apparatus. UV spectra were recorded on a Hitachi U-3210 spectrometer. IR spectra were recorded on a HORIBA FT-210 fourier transform infrared spectrometer. HRESI-MS spectra were recorded on a JEOL JMS-T100LC spectrometer. NMR spectra were recorded on a JEOL JNM-A400 spectrometer using TMS as an internal reference. Optical rotations were measured with a Perkin-Elmer 241 polarimeter.

Preparation of D-Amicetose (5)

Kigamicin A (81.1 mg, 0.122 mmol) in THF (2.5 ml) and 1 N-HCl (1.0 ml) was stirred at room temperature for 18 hours. After removal of THF by evaporation, the residue was dissolved with water (30 ml) and ethyl acetate (30 ml) and shaken vigorously. The aqueous layer was neutralized with Ag_2CO_3. The resulting precipitate was filtered off and the filtrate was concentrated *in vacuo* to afford oily material. This material was subjected to silica gel column chromatography using $CHCl_3/Me_2CO=1/1$ as an eluent. The fractions showing positive color reaction to anisaldehyde-H_2SO_4 at Rf 0.33 ($CHCl_3/Me_2CO=1/1$) on a TLC were collected to afford 14.5 mg (90% yield) of colorless syrup. HRESI-MS *m/z* found 155.0701 $(M+Na)^+$, calcd for $C_6H_{12}O_3Na$ 155.0684: $[\alpha]_D^{22}$ +42.5° (*c* 0.7, Me_2CO), lit. [4]; $[\alpha]_D^{22}$ +43.6° (*c* 1.2, Me_2CO): TLC (silica gel) Rf 0.33 (solvent system; $CHCl_3/Me_2CO=1/1$).

Preparation of Aglycon (4)

The organic layer above-mentioned was concentrated *in vacuo* and subjected to Sephadex LH-20 column chromatography using $MeOH/CHCl_3=5/1$ as an eluent. Fractions containing **4** were collected and evaporated *in vacuo* to afford 51 mg (76%) of yellowish powders. Yellow crystals were obtained from $MeOH/H_2O$. mp 230~235°C (dec.): $[\alpha]_D^{24}$ −438° (*c* 0.3, $CHCl_3$): UV λ_{max} (MeOH) nm (ε) 219 (32,900), 253 (32,200), 355 (14,300): IR ν_{max} cm^{-1} (KBr) 3495, 2885, 1645, 1610, 1465, 1440, 1275, 1200, 1090: HRESI-MS *m/z* found 574.1336 $(M+Na)^+$, calcd for $C_{28}H_{25}NO_{11}Na$ 574.1325: ^{13}C NMR ($CDCl_3/CD_3OD=2/1$) 182.8 (C-10), 164.6 (C-3), 163.1 (C-16), 158.1 (C-5), 149.8 (C-8), 143.9 (C-17), 140.5 (C-22), 135.7 (C-24), 130.6 (C-18), 129.8 (C-19), 118.7 (C-11), 118.5 (C-23), 117.8 (C-4), 111.7 (C-9), 110.4 (C-6), 110.0 (C-7), 92.1 (C-26), 90.9 (C-28), 72.6 (C-20), 70.1 (C-14), 69.7 (C-15), 64.0 (C-1), 61.6 (C-12), 41.6 (C-2), 39.9 (C-25), 36.0 (C-21), 32.2 (C-13), 22.0 (C-27).

Preparation of Disaccharide (6)

Kigamicin D (53.3 mg, 0.056 mmol) in THF (1.25 ml) and 0.2 N-HCl (0.5 ml) was stirred at room temperature for 20 hours. After removal of THF by evaporation, the residue was dissolved with water (20 ml) and ethyl acetate (20 ml) and the mixture was shaken vigorously. The aqueous layer was neutralized with Ag_2CO_3. The resulting precipitates were filtered off and the filtrate was concentrated *in vacuo* to afford 12 mg of crude powder. This material was subjected to silica gel column chromatography using $CHCl_3/Me_2CO=1/1$ as an eluent. The fractions showing positive color reaction to anisaldehyde-H_2SO_4 at Rf 0.50 ($CHCl_3/Me_2CO=1/1$) on a TLC were collected and concentrated to afford 3.1 mg of white powders. Colorless needles were obtained from EtOAc/*n*-hexane. mp 133~136°C: $[\alpha]_D^{22}$ +32.5° (*c* 0.2, Me_2CO): HRESI-MS *m/z* found 299.1464 $(M+Na)^+$, calcd for $C_{13}H_{24}O_6Na$ 299.1471.

Preparation of Trisaccharide (7)

Kigamicin D (100 mg) in THF (2.5 ml) and 0.2 N-HCl (0.5 ml) was stirred at room temperature for 48 hours. After removal of THF by evaporation, the residue was dissolved with water (40 ml) and ethyl acetate (40 ml). The aqueous layer was neutralized with Ag_2CO_3. The resulting precipitates were filtered off and the filtrate was concentrated *in vacuo* to afford 20 mg of crude powder. This material was subjected to silica gel column chromatography using toluene/$Me_2CO=3/2$ as an eluent. The fractions showing positive color reaction to anisaldehyde-H_2SO_4 at Rf 0.28 (toluene/$Me_2CO=3/2$) on a TLC were collected and concentrated to afford 11 mg of white powders. Colorless needles were obtained from ether/n-hexane. mp 161~163°C: $[\alpha]_D^{22}$ +6.2° (*c* 0.2, Me_2CO): HRESI-MS *m/z* found 443.2244 $(M+Na)^+$, calcd for $C_{20}H_{36}O_9Na$ 443.2257.

X-Ray Structure Analysis of 1

Crystals of **1** were obtained from a hot MeOH/H_2O solution. A yellow plate crystal of 0.01×0.15×0.30 mm was mounted on a glass fiber. All measurements were made on a Rigaku AFC7R diffractometer with graphite monochromated Cu-Kα radiation. Crystal data: Empirical formula; $C_{34}H_{35}NO_{13}$, Formula weight; 665.65, Crystal system; orthorhombic, Space group; $P2_12_12_1$, Lattice parameters; a=12.097(2) Å, b=32.337(3) Å, c=8.053(2) Å, Volume; 31501(1) Å^3, Z value; 4, D_{calc}; 1.403 g/cm^3, μ(CuKα); 9.2 cm^{-1}, T; 293 K. The structure was solved by a direct method (SIR92). Final R and wR were 0.06 and 0.157 for 2572 observed reflections, respectively.

X-Ray Structure Analysis of 7

A colorless needle crystal of **7** (0.46×0.11×0.07 mm) was mounted in a loop. All measurements were made on a Bruker SMART APEX diffractometer with graphite monochromated Cu-Kα radiation. Crystal data: Empirical formula; $C_{20}H_{36}O_9$, Formula weight; 420.49, Crystal system; monoclinic, Space group; C2, Lattice parameters; a=60.606(6) Å, b=5.0208(5) Å, c=14.9319(14) Å, β=101.659(4)°, Volume; 4449.9(7) Å^3, Z value; 8, D_{calc}; 1.255 g/cm^3, (CuKα); 0.819 mm^{-1}. The reflection data were collected at 90 K using the ω scans. The structure was solved by a direct method (SHELXS-97). Final R and wR were 0.088 and 0.2163 for 5771 observed reflections, respectively.

Acknowledgements The authors wish to thank Dr. Kenji Yoza of Bruker AXS K.K. for the measurement of X-ray data of **7**. This paper is supported by a Grant for Medical Frontier Program from the Ministry of Health, Labor and Welfare of Japan.

References

1. Kunimoto S, Lu J, Esumi H, Yamazaki Y, Kinoshita N, Honma Y, Hamada M, Ohsono M, Ishizuka M, Takeuchi T. Kigamicins, novel antitumor antibiotics. I. Taxonomy, isolation, physico-chemical properties and biological activities. J Antibiot 56: 1004–1011 (2003)
2. Kunimoto S, Someno T, Yamazaki Y, Lu J, Esumi H, Naganawa H. Kigamicins, novel antitumor antibiotics. II. Structure determination. J Antibiot 56: 1012–1017 (2003)
3. Lu J, Kunimoto S, Yamazaki Y, Kaminishi M, Esumi H. Kigamicin D, a novel anticancer agent based on a new anti-austerity strategy targeting cancer cells, tolerance to nutrient starvation. Cancer Sci 95: 547–552 (2004)
4. Stevens CL, Blumbergs P, Wood DL. Stereochemical idenyification and synthesis of amicetose and the stereochemical identification of rhodinose and the sugar from streptolydigin. J Am Chem Soc 86: 3592–3594 (1964)
5. Berti G, Caroti P, Catelani G, Monti L. Synthesis of D-amicetose and L-rhodinose from L-glutamic acid. Carbohydr Res 124: 35–42 (1983)
6. BLindenbacher F, Reichstein T. Synthese der L-oleandrose. Helv 31: 2061–2064 (1948)
7. Els H, Celmer WD, Murai K. Oleandomycin (PA-105). II. Chemical characterization (I). J Am Chem Soc 80: 3777–3782 (1958)
8. Vischer E, Reichstein T. Synthese des D-oleandrose. Helv 27: 1332–1345 (1944)
9. Nakagawa A, Ōmura S, Kusida K, Shimizu H, Lukacs G. Structure of cervinomycin, a novel xanthone antibiotic active against anaerobe and mycoplasma. J Antibiot 40: 301–319 (1987)
10. Kobayashi K, Nishino C, Ohya J, Sato S, Mikawa T, Shiobara Y, Kodama M. Actinoplanones, C, D, E, F and G, new cytotoxic polycyclic xanthones from *Actinoplanes* sp. J Antibiot 41: 741–750 (1988)
11. Maiese WM, Lechevalier MP, Korshalla J, Goodman J, Wildey MJ, Kuck N, Greenstein M. LL-E19085α, A novel antibiotic from *Micromonospora Citrea*: Taxonomy, fermentation and biological activity. J Antibiot 42: 846–851 (1989)
12. Maiese WM, Korshalla J, Goodman J, Torrey MJ, Kantor S, Labeda DP, Greenstein M. Simaomiin (LL-D42067), a novel antibiotic from *Actinomadura Madurae*. I. Taxonomy, fermentation and biological activity. J Antibiot 43: 1059–1063 (1990)
13. Ojiri K, Nishioka H, Torigoe K, Nakajima S, Kawamura K, Suda H. Antitumor antibiotic BE-13793X and its derivatives BE-13793XA manufacture with streptoverticillium. Jap Kokai Tokkyo Koho JP07,258,93 [95,258,93]
14. Herbert K, Fehlhaber HW, Mather CM, Upadhyay DJ, Coutinho LEL, Ganguli BN, Blumbach J. Novel antibiotic MSO901809H and MSO901809H, and their production. Eur Pat Appl EP512,522
15. Kondo K, Eguchi T, Kakinuma K, Mizoue K, Qiao YF. Structure and biosynthesis of FD-594; a new antitumor antibiotic. J Antibiot 51: 288–295 (1998)